Bulg. J. Phys. **42** (2015) 477–484

Mechanism of Termination of Negative-Parity Bands

G.G. Adamian[1], **N.V. Antonenko**[1], **H. Lenske**[2]
[1]Joint Institute for Nuclear Research, 141980 Dubna, Russia
[2]Institut für Theoretische Physik der Justus–Liebig–Universität, D-35392 Giessen, Germany

Received *14 October 2015*

Abstract. The cluster approach is applied to study the mechanism of termination of the lowest negative-parity bands in even-even nuclei. The new method is suggested for the verification of the cluster interpretation of the band termination.

PACS codes: 21.60.Ev, 21.60.Gx

1 Introduction

The low-lying negative-parity states observed in pre-actinides, actinides, medium-mass isotopes, and light nuclei are definitely related to reflection-asymmetric shapes [1]. There are several approaches based on the assumption that the reflection-asymmetric shape is the consequence of the octupole deformation or clustering in nuclei [2–13]. In the framework of the cluster model [8–13] the dependencies of parity splitting and multipole $E1$, $E2$, and $E3$ transition moments on spin in the alternating parity bands built on the ground states of even and odd medium-mass and heavy nuclei have been successfully described. This collective model is based on the assumption that the reflection-asymmetric shape is a consequence of alpha clustering in nuclei. The energetically favorable ^{4}He-cluster configuration $^AZ \rightarrow ^{A-4}(Z-2)+^4$He, two touching clusters, has been used in order to describe the properties of the low-lying negative-parity rotational states.

If the cluster model [8–13] gives a good quantitative explanation of the observed properties of the low-lying negative-parity bands, this collective model can serve as a good ground for the description and better understanding of the mechanism of termination of these bands. The cluster configuration is located in the minimum of potential pocket of the cluster-cluster interaction potential. Because the centrifugal potential acts repulsively and enforces this minimum, for values J larger than the critical angular momentum J_{max}, the pocket vanishes (its

depth becomes zero) and di-cluster system becomes unbound and easily decays into two fragments. However, even at $J \leq J_{max}$ the cold (the internal excitation energy is zero) rotating dinuclear system (DNS) decays into two fragments (α-decay) by tunneling through the potential barrier. So, at high spins the $E2$-transition between negative-parity states competes with α-decay. With increasing J the α-decay time $T_\alpha(J)$ becomes comparable and then smaller than the $\gamma-$transition time $T_\gamma(J)$. One can expect that the terminating spins J_{term} [$J_{term} < J_{max}$] for the ${}^AZ \rightarrow {}^{A-4}(Z-2)+{}^4$He cluster configuration is determined from the condition

$$T_\alpha(J_{term}) \ll T_\gamma(J_{term}). \quad (1)$$

Thus, at $J \geq J_{term}$ the cold cluster configuration ${}^AZ \rightarrow {}^{A-4}(Z-2)+{}^4$He is unstable and, correspondingly, the related low-lying negative-parity band does not exist. The negative-parity band disappears upon reaching this terminating state with $J = J_{term}$. One can say that the physical origin of the termination of negative-parity rotational band built on the ground state is the alpha-decay which observations allows us to verify whether the cluster interpretation is suitable for the low-lying negative-parity states.

2 Model

The cluster model is based on the assumption that the reflection-asymmetric shapes are produced by the collective motion of the nuclear system in the mass (charge) asymmetry coordinate $\eta = (A_1 - A_2)/(A_1 + A_2)$ ($\eta_Z = (Z_1 - Z_2)/(Z_1 + Z_2)$), where A_1 (Z_1) and A_2 (Z_2) are the mass (charge) numbers, respectively, clusters. Here the molecular-like cluster systems are two touching clusters with a relative distance about $R_m = R_1 + R_2 + 0.5$ fm (the touching configuration), which corresponds to the minimum of the shallow effective cluster-cluster interaction potential. The relative weights of each cluster and clusterless (mononucleus) components in the wave function $\Psi_J(\eta)$ are determined by solving the stationary Schrödinger equation

$$(T + U)\Psi_J(\eta) = E_J\Psi_J(\eta)$$

in mass (charge) asymmetry coordinate with the kinetic T and potential

$$U(\eta, R_m, J, \beta_i) = B_1 + B_2 + V(R_m, J, \beta_i)$$

energies. Here, U is equal to the sum of the binding energies B_i ($i = 1, 2$) of clusters and the cluster-cluster interaction V which contains the rotational energy. Since the potential energy is invariant under the inversion $\eta \rightarrow -\eta$, every non-degenerate eigenfunction $\Psi_J(\eta)$ has a definite parity. The rotational states are built on the vibrational states in η. In the case of the even-even nuclei we

have a set of states with $J^\pi = 0^+, 1^-, 2^+, 3^-, 4^+, ...$; i.e., the positive and negative rotational bands are built on the lowest even and odd states in η, respectively. So, the positive and negative parity states are treated on the same footing [8–13]. Note that the low-lying positive-parity rotational states are mainly described by the mononucleus component (clusterless configuration).

Because the energies of cluster configurations with a light cluster heavier than the α-particle increase rapidly with decreasing η (η_Z), the energetically favorable ^{4}He-cluster configuration $^AZ \rightarrow ^{A-4}(Z-2)+^4$He gives the main contribution in the wave function $\Psi_J(\eta)$ [8–13]. In the low-lying negative-parity rotational states with high spins, the value of the α-particle spectroscopic factor becomes close to unity. At small spins, the spectroscopic factor is less than unity. Thus, it could be argued that the reflection-asymmetric shape, especially at the high spins, is a consequence of alpha clustering in the nucleus.

To calculate the termination spin J_{term}, we use the nucleus-nucleus interaction potential [8–14]

$$V(R, J, \beta_i) = V_C + V_N + \hbar^2 J(J+1)/(2\Im). \quad (2)$$

It is given as the sum of the Coulomb potential V_C, the nuclear potential V_N and the centrifugal potential (last summand) with the moment of inertia $\Im$ of the DNS formed. In our notations R, μ, and β_i $(i = 1, 2)$ are the relative distance between the centers of clusters, reduced mass parameter, and the quadrupole deformation parameters of the clusters, respectively. For the nuclear part, we use the double-folding formalism with the Skyrme-type effective density-dependent nucleon-nucleon interaction [14]. The relative orientation of the deformed cluster in the cluster configuration follows the minimum of the potential energy which results in the sphere-to-pole or pole-to-pole orientation. The absolute values of the quadrupole deformation parameters β_i of the deformed nuclei are taken from Ref. [15]. For the double magic and semi-magic nuclei, we take $\beta_i = 0$.

The value of $\Im$ is calculated in the sticking limit as

$$\Im(R, \beta_i) = k_0(\Im_1 + \Im_2 + \mu R^2). \quad (3)$$

For large angular momenta J, the moments of inertia $\Im_i$ $(i = 1, 2)$ of the DNS nuclei are obtained in the rigid body approximation. As known from the experimental study, the moments of inertia of strongly deformed nuclear states are close to 85% of those in the rigid body limit [16]. We also set k_0=0.85 in our calculations.

For the ^{4}He + ^{70}Se system, the nucleus-nucleus interaction potential V versus R is presented in Figure 1 at different values of angular momentum J. The antisymmetrization between nucleons belonging to different clusters is regarded by a density dependence of the nucleon-nucleon force which gives a repulsive core in the cluster-cluster interaction potential. As a result of the

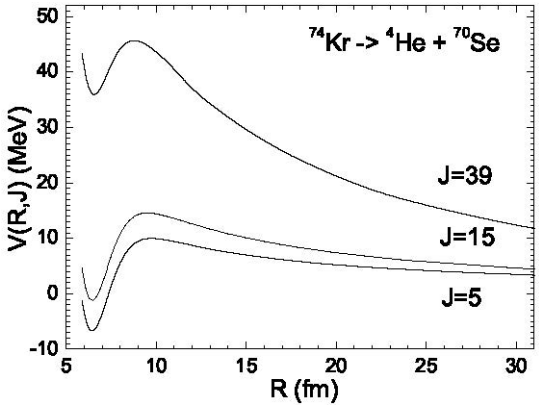

Figure 1. Nucleus-nucleus interaction potential for the ^{4}He + ^{70}Se system at indicated angular momenta.

density-dependent nucleon-nucleon interaction used in the calculation of V, a repulsive core appears which prevents the motion to smaller R and reflects the action of the Pauli principle. Due to the sum of the repulsive Coulomb and centrifugal summands with the attractive nuclear one in Eq. (2), the nucleus-nucleus potential has a potential pocket with a minimum situated at the distance $R = R_m \approx R_1(\beta_1) + R_2(\beta_2) + 0.5$ fm, where R_i are the radii of clusters. The cluster system is localized in the minimum of this pocket at $R = R_m$. The position of the Coulomb barrier corresponds to $R = R_b \approx R_m + (3.2 - 3.8)$ fm at $J = 0$ in the cluster configurations considered. Then the depth of the potential pocket is

$$B_R^{qf}(J) = V(R_b, J, \beta_i) - V(R_m, J, \beta_i). \quad (4)$$

The barrier B_R^{qf} prevents the cluster system decay in R. So, the stability of the cluster system is governed by the value of B_R^{qf}. The depth B_R^{qf} of the potential pocket decreases with increasing J because of the growth of repulsive centrifugal part of the nucleus-nucleus potential (2) and vanishes at $J > J_{max}$. For the ^{4}He + ^{70}Se system, J_{max}=45. One can see in Figure 1 that the value of B_R^{qf} decreases by 6.9 MeV with increasing J from 5 to 39.

Using the values of $\Im$ and the electric quadrupole moment of the DNS ($Q_2^{(c)}(i)$ $(i = 1, 2)$ are the quadrupole moments of the DNS nuclei) [17]

$$Q_2^{(c)} = 2e\frac{A_2^2 Z_1 + A_1^2 Z_2}{A^2} R_m^2 + Q_2^{(c)}(1) + Q_2^{(c)}(2),$$

we obtain the energy $E_\gamma(J \to J-2) = J(J+1)/(2\Im) - (J-2)(J-1)/(2\Im) = (2J-1)/\Im$ and the time $T_\gamma(J)$ of the collective $E2$-transition between the

rotational states with J and $J-2$ as in Ref. [15]:

$$T_\gamma(J) = \frac{408.1}{5/(16\pi)(Q_2^{(c)})^2(E_\gamma(J \to J-2))^5}, \tag{5}$$

where E_γ is in units of keV, $Q_2^{(c)}$ in $10^2(e\ \mathrm{fm}^2)$ and T_γ in s.

The process which competes with γ emission is tunneling through the barrier in R (α-decay). By employing the WKB-approach, the tunneling time through the barrier in R is estimated as

$$T_\alpha(J) = \frac{2\pi}{\omega_m(J)}(1+\exp[2S_\alpha(J)/\hbar]), \tag{6}$$

where

$$S_\alpha(J) = \int_{R_m}^{R_{ex}} dR[2\mu(V(R,J,\beta_2) - E_{\mathrm{c.m.}})]^{1/2}$$

is the classical action in R, R_{ex} is the external turning point, and ω_m is the assault frequency in the potential pocket at given value of J.

3 Calculation Results

The condition (1) sufficiently restricts the interval of angular momenta at which one can identify states of the negative-parity band. As seen from (5), the value of T_γ mainly depends on J through E_γ. The angular momentum dependence of T_α are defined by the angular momentum dependence of the Coulomb barrier. The value of barrier B_{qf}^R decreases with increasing contribution of the repulsive centrifugal part in Eq. (2) (see Figure 1). For example, the values T_γ

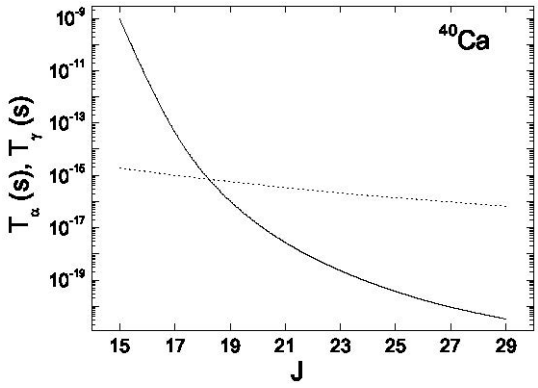

Figure 2. Times of $E2-$transition and α-decay as the functions of angular momentum J for the indicated nucleus.

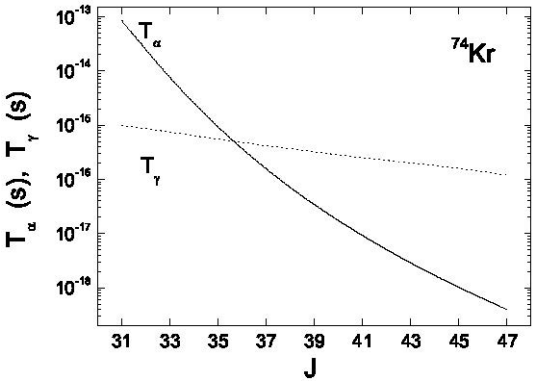

Figure 3. Times of $E2-$transition and α-decay as the functions of angular momentum J for the indicated nucleus.

and T_α as the functions of J are presented in Figures 2 and 3 for the systems ^{40}Ca$\rightarrow^{4}$He+^{36}Ar and ^{74}Kr$\rightarrow^{4}$He+^{70}Se. The two curves cross each other and the condition $T_\alpha \ll T_\gamma$ is valid only at high J when the value of B^R_{qf} considerably decreases. Near this crossing point the γ- and α-decay probabilities becomes comparable. Thus, one can see from the analysis of Figures 2 and 3 that the α-cluster nature of the negative-parity states can be identified by measuring the rotational γ-quanta in coincidence with the α-decay fragments at J corresponding to the vicinity of the crossing point in the nuclei ^{40}Ca and ^{74}Kr.

The nucleus-nucleus interaction potential (2) and condition (1) are applied to the prediction of the termination spins J_{term} of negative-parity bands built on the ground state in the nuclei ^{20}Ne, ^{24}Mg, ^{28}Si, ^{32}S, ^{36}Ar, ^{40,42}Ca, ^{44}Ti, ^{54}Cr, ^{62}Zn, ^{74}Kr, and ^{102}Pd (Figure 4). For example, we obtain J_{term}=19, 21, 29, 39, and 51 for the nuclei ^{40}Ca$\rightarrow^{36}$Ar+^{4}He, ^{44}Ti$\rightarrow^{40}$Ca+^{4}He, ^{62}Zn$\rightarrow^{58}$Ni+^{4}He, ^{74}Kr$\rightarrow^{70}$Se+^{4}He, and ^{102}Pd$\rightarrow^{98}$Ru+^{4}He, respectively (see Figures 2–4). Note that in the nuclei ^{44}Ti, ^{62}Zn, ^{74}Kr, and ^{102}Pd, the presently measured highest spin values within negative-parity band built on the ground state are $J^\pi = 13^-$, 13^-, 35^-, and 21^-, respectively [18, 19]. They are always smaller than our predicted J_{term}. In Figure 4, the J_{term} is almost linear dependent on the atomic number Z of nucleus, increasing by the factor of ~ 4.6 from $Z = 10$ to $Z = 46$. The differences between J_{term} in these α-cluster configurations arise due to the differences of their $B^{qf}_R(J = 0)$ and moments of inertia [through the differences of R_m and R_b]. The deformation of the heavy nucleus comes also into the play through the R_m and R_b. For instance, for nuclei ^{42}Ca and ^{44}Ti, the barriers and moments of inertia [$\beta_2(^{38}\text{Ar})=\beta_2(^{40}\text{Ca})=0$] of their α-cluster configurations are similar that results in the same termination spins, J_{term}=21. The gain in $B^R_{qf}(J = 0)$ for ^{36}Ar with respect to ^{42}Ca or ^{44}Ti compensates the loss in the moment of inertia leading to the same J_{term}.

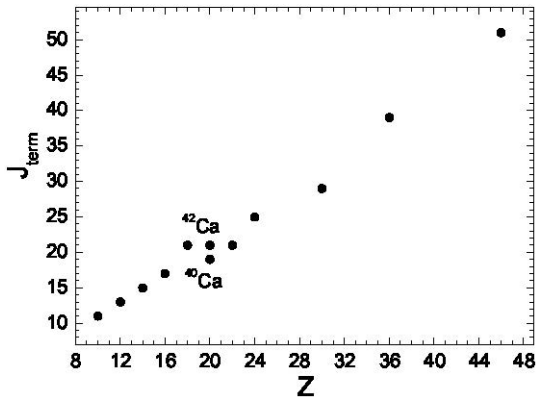

Figure 4. The termination spin as a function of atomic number.

After the γ-emission ($E1$ or $E2$) from the negative-parity state with $J = J_{term} - 2$ [the positive-parity state with $J = J_{term} - 1$ or $J = J_{term} - 3$] to the negative-parity state with $J = J_{term} - 4$ [$J_{term} - 2$ or $J = J_{term} - 4$], the $^{A}Z \rightarrow^{A-4} (Z-2)+^{4}$He cluster configuration can decay into two fragments because the decay its probability is rather high at J in the vicinity of J_{term}. By measuring the γ-emission in coincidence with decay fragments of the alpha-cluster system, one can obtain the direct prove of the cluster feature of the negative-parity states. We think this correlation states can be studied with a large gamma-ray detector array and an additional detector setup to register the fragments. One can also measure the average kinetic energy of the decay fragments and compare with the theoretical one.

4 Conclusions

Applying the cluster interpretation to the description of the lowest negative-parity band, the terminating spins $J = J_{term}$ for the even-even nuclei ^{20}Ne, ^{24}Mg, ^{28}Si, ^{32}S, ^{36}Ar,^{40,42}Ca, ^{44}Ti, ^{54}Cr, ^{62}Zn, ^{74}Kr, and ^{102}Pd were determined. We predicted that the physical origin of the termination of negative-parity band is the decay of the alpha-cluster configuration into two fragments. To verify in the experiments the cluster origin of the low-lying negative parity states, one could suggest to measure the γ-emission from the negative-parity state with $J = J_{term} - 2$ [positive-parity state with $J = J_{term} - 1$ or $J = J_{term} - 3$] to the lower negative-parity state in coincidence with decay fragments of the corresponding alpha-cluster configuration. Since the alpha-cluster spectroscopic factor in the state with even spin J is smaller than in the state with odd spin $J - 1$ or $J + 1$, the lowest negative-parity band must be shorter than the positive-parity band built on the ground state.

Acknowledgments

G.G.A. and N.V.A. acknowledge the partial financial support from the HIC for FAIR guest funds of the Justus-Liebig University Giessen and Heisenberg-Landau programme (Dubna). This work was partly supported by RFBR.

References

[1] L.P. Gaffney *et al.* (2013) *Nature* **497** 199.

[2] N. Minkov, S. Drenska, M. Strecker, W. Scheid, and H. Lenske (2012) *Phys. Rev. C* **85** 034306; D. Bonatsos, A. Martinou, N. Minkov, S. Karampagia, and D. Petrellis (2015) *Phys. Rev. C* **91** 054315.

[3] O.F. Nemetz, V.G. Neudachin, A.T. Rudchik, Yu.F. Smirnov, and Yu.M. Tchuvil'sky (1988) *Nucleon Clusters in Atomic Nuclei and Multi-Nucleon Transfer Reactions*, Naukova Dumka, Kiev.

[4] B. Buck, A.C. Merchant, S.M. Perez, and H.E. Seals (2005) *J. Phys. G: Nucl. Part. Phys.* **31** 1499.

[5] J. Darai, J. Cseh, and D.G. Jenkins (2012) *Phys. Rev. C* **86** 064309.

[6] M. Spieker, S. Pascu, A. Zilges, and F. Iachello (2015) *Phys. Rev. Lett.* **114** 192504.

[7] A. Volya and Yu.M. Tchuvilsky (2015) *Phys. Rev. C* **91** 044319.

[8] T.M. Shneidman, G.G. Adamian, N.V. Antonenko, R.V. Jolos, and W. Scheid (2002) *Phys. Lett.* **B526** 322; (2003) *Phys. Rev. C* **67** 014313.

[9] G.G. Adamian, N.V. Antonenko, R.V. Jolos, and T.M. Shneidman (2004) *Phys. Rev. C* **70** 064318; T.M. Shneidman, G.G. Adamian, N.V. Antonenko, and R.V. Jolos (2006) *Phys. Rev. C* **74** 034316.

[10] T.M. Shneidman, G.G. Adamian, N.V. Antonenko, R.V. Jolos, and S.-G. Zhou (2015) *Phys. Rev. C* **92** 034302.

[11] G.G. Adamian, N.V. Antonenko, R.V. Jolos, Yu.V. Palchikov, and W. Scheid (2003) *Phys. Rev. C* **67** 054303; G.G. Adamian, N.V. Antonenko, R.V. Jolos, Yu.V. Palchikov, W. Scheid, and T.M. Shneidman (2004) *Phys. Rev. C* **69** 054310.

[12] S.N. Kuklin, T.M. Shneidman, G.G. Adamian, and N.V. Antonenko (2012) *Eur. Phys. J. A* **48** 48.

[13] G.G. Adamian, N.V. Antonenko, and W. Scheid (2012) *Lect. Notes Phys.* **848**, Clusters in Nuclei, Vol. 2, ed. Christian Beck; Springer-Verlag, Berlin, p. 165.

[14] G.G. Adamian, N.V. Antonenko, R.V. Jolos, S.P. Ivanova, and O.I. Melnikova (1996) *Int. J. Mod. Phys. E* **5** 191.

[15] S. Raman, C.W. Nestor, Jr, and P. Tikkanen (2001) *At. Data Nucl. Data Tables* **78** 1.

[16] J. Dudek (1992) *Prog. Part. Nucl. Phys.* **28** 131.

[17] T.M. Shneidman, G.G. Adamian, N.V. Antonenko, S.P. Ivanova, and W. Scheid (2000) *Nucl. Phys.* **A671** 119.

[18] http://www.nndc.bnl.gov/.

[19] J.J. Valiente-Dobón *et al.* (2005) *Phys. Rev. Lett.* **95** 232501.